Bollettino di Geofisica Teorica ed Applicata Vol. 54, n. 4, pp. 367-384; December 2013
DOI 10.4430/bgta0108

Fully dynamic approach for GOCE precise orbit determination

S. Casotto[1,2], F. Gini[2], F. Panzetta[2] and M. Bardella[1]

[1] *Dipartimento di Fisica e Astronomia, Università di Padova, Italy*
[2] *Centro Interdipartimentale di Studi e Attività Spaziali (CISAS), Università di Padova, Italy*

(Received: January 15, 2013; accepted: July 10, 2013)

ABSTRACT Gravity field and steady-state Ocean Circulation Explorer (GOCE) was launched in 2009 at 250 km altitude to recover the Earth's static gravity field. As part of the GOCE-Italy project, we carried out GPS-based, fully dynamic Precise Orbit Determination (POD) of GOCE for daily arcs covering about 500 days (November 1, 2009 - May 31, 2011). Three sequences were defined and implemented with the software NAPEOS (ESA/ESOC). A first sequence uses the orbit propagated from the previous day as an a-priori orbit but, to avoid one-day failures compromising all the subsequent POD processing chain, other two sequences were built using the official kinematic Precise Science Orbits (PSO) as a-priori orbits. For those days where the sequences based on the PSO gave less accurate results, or even failure, the a-priori orbit propagated from the previous day was employed. Results show an average post-fit RMS of zero-difference phase measurements below 10 mm for about 90% of the daily arcs. Most orbits compare to less than 6 cm 3D RMS with respect to the official kinematic and reduced-dynamics PSO orbits. To evaluate the quality of the POD results, 366 overlapping arcs of 5 hours were compared, showing an average distance below 1 cm.

Key words: GOCE; Precise Orbit Determination (POD); GPS; Fully Dynamic POD.

1. Introduction

The Gravity field and steady-state Ocean Circulation Explorer (GOCE) (ESA, 1999) is the first Earth explorer core mission of the European Space Agency (ESA). It was launched on March 17, 2009 from Plesetsk, Russia. The mission is dedicated to high-resolution gravity field extraction and carries, as primary instrument, a three-axis gradiometer for determining the gravity field with an unprecedented accuracy of 1 mGal and the geoid with an accuracy of 1 cm, both at a spatial resolution of 100 km (Drinkwater *et al.*, 2007). In addition the mission is equipped with two 12-channel dual-frequency LAGRANGE GPS/GLONASS Satellite-to-Satellite Tracking Instruments (SSTIs) consisting of an independent receiver and antenna each. The measurements of the main onboard GPS receiver (SSTI-A) allow for Precise Orbit Determination (POD) of the satellite and for gravity field recovery of the low degree and order terms.

POD for the GOCE satellite is one task of the GOCE-Italy group, an ESA project endorsement funded by the Agenzia Spaziale Italiana (ASI). Based on the GPS data availability

GOCE orbits were estimated at the University of Padua and this was performed with a densely-parameterized, fully dynamic POD approach.

The results discussed subsequently were all obtained from 1 Hz data of the SSTI-A (RINEX data) in the time interval from November 1, 2009 to May 31, 2011 (496 days of data availability).

General GOCE data information employed to perform the POD is provided in Section 2, the dynamical model and the estimated and fixed parameters adopted during the POD process are described in Section 3, the software and the POD chains implemented are presented in Section 4. In Section 5 the GOCE orbit results for the 496-day period are then illustrated and discussed. Conclusions are reported in Section 6.

2. GOCE useful data for POD processing

GOCE POD was performed using as the main input data GOCE GPS phase observables, International GNSS Service (IGS) (Dow *et al.*, 2009) final GPS orbits and clock solutions, GOCE GPS antenna information in ANTEX format, GOCE radiation cross-section area, aerodynamic cross-section area, and attitude information.

GOCE GPS raw observations are collected and delivered at 1 Hz by GOCE SSTI-A, which consists of a 12-channel dual-frequency LAGRANGE (Laben GNSS Receiver for Advanced Navigation, Geodesy and Experiments) GPS/GLONASS receiver (the GOCE flight model only tracks GPS measurements) and an L-band antenna; SSTI-B is a fully redundant backup receiver. The internal clock of the GOCE LAGRANGE receiver is not steered to integer seconds with

Table 1 - GOCE SSTI data availability: daily reports over the period November 1, 2009 - May 31, 2011.

RINEX

2009	1	2	3	4	5	6	7	8	9	10	11	12	13	14	15	16	17	18	19	20	21	22	23	24	25	26	27	28	29	30	31
November	305	306	307	308	309	310	311	312	313	314	315	316	317	318	319	320	321	322	323	324	325	326	327	328	329	330	331	332	333	334	
December	335	336	337	338	339	340	341	342	343	344	345	346	347	348	349	350	351	352	353	354	355	356	357	358	359	360	361	362	363	364	365
2010																															
January	1	2	3	4	5	6	7	8	9	10	11	12	13	14	15	16	17	18	19	20	21	22	23	24	25	26	27	28	29	30	31
February	32	33	34	35	36	37	38	39	40	41	42	43	44	45	46	47	48	49	50	51	52	53	54	55	56	57	58	59			
March	60	61	62	63	64	65	66	67	68	69	70	71	72	73	74	75	76	77	78	79	80	81	82	83	84	85	86	87	88	89	90
April	91	92	93	94	95	96	97	98	99	100	101	102	103	104	105	106	107	108	109	110	111	112	113	114	115	116	117	118	119	120	
May	121	122	123	124	125	126	127	128	129	130	131	132	133	134	135	136	137	138	139	140	141	142	143	144	145	146	147	148	149	150	151
June	152	153	154	155	156	157	158	159	160	161	162	163	164	165	166	167	168	169	170	171	172	173	174	175	176	177	178	179	180	181	
July	182	183	184	185	186	187	188	189	190	191	192	193	194	195	196	197	198	199	200	201	202	203	204	205	206	207	208	209	210	211	212
August	213	214	215	216	217	218	219	220	221	222	223	224	225	226	227	228	229	230	231	232	233	234	235	236	237	238	239	240	241	242	243
September	244	245	246	247	248	249	250	251	252	253	254	255	256	257	258	259	260	261	262	263	264	265	266	267	268	269	270	271	272	273	
October	274	275	276	277	278	279	280	281	282	283	284	285	286	287	288	289	290	291	292	293	294	295	296	297	298	299	300	301	302	303	304
November	305	306	307	308	309	310	311	312	313	314	315	316	317	318	319	320	321	322	323	324	325	326	327	328	329	330	331	332	333	334	
December	335	336	337	338	339	340	341	342	343	344	345	346	347	348	349	350	351	352	353	354	355	356	357	358	359	360	361	362	363	364	365
2011																															
January	1	2	3	4	5	6	7	8	9	10	11	12	13	14	15	16	17	18	19	20	21	22	23	24	25	26	27	28	29	30	31
February	32	33	34	35	36	37	38	39	40	41	42	43	44	45	46	47	48	49	50	51	52	53	54	55	56	57	58	59			
March	60	61	62	63	64	65	66	67	68	69	70	71	72	73	74	75	76	77	78	79	80	81	82	83	84	85	86	87	88	89	90
April	91	92	93	94	95	96	97	98	99	100	101	102	103	104	105	106	107	108	109	110	111	112	113	114	115	116	117	118	119	120	
May	121	122	123	124	125	126	127	128	129	130	131	132	133	134	135	136	137	138	139	140	141	142	143	144	145	146	147	148	149	150	151

LEGEND

Available
Not available
To be discarded
SSTI Anomaly
UTC Missing Epochs; usable
UTC Missing Epochs; not Usable

some jumps of 20 ms. For the POD process, GOCE GPS data covering the time interval from November 1, 2009 (beginning of the operational phase) to May 31, 2011 were obtained in RINEX 2.20 format (file type SST_RIN_1b) through EOLi-SA (Earth Observation Link - Stand Alone) (EOLI-SA, 2012), an interactive tool to view and order products from ESA's Earth observation catalogues.

SSTI data availability over the considered period is shown in more detail in Table 1. Note that the data set is not continuous and several intervals or single epochs are missing, generally due to onboard system failures or anomalies, as reported in monthly reports available on the GOCE Monthly Statistics website (GOCE, 2013).

Official GOCE kinematic PSO solutions were used as a-priori orbits for the smoothing of raw observations during the POD process and as a term of comparison for the estimated orbits. These official orbits include positions at 1 s sampling (file types SST_PSO_2) for the kinematic orbits and positions and velocities at 10 s sampling for the reduced-dynamics orbits. They are generated at the Astronomical Institute of the University of Bern (AIUB, Bern, Switzerland) with the support of the Institute of Astronomical and Physical Geodesy (IAPG, Technische Universität München, München, Germany) (Bock *et al.*, 2007; Visser *et al.*, 2009). The official PSO solutions are provided with an accuracy of 2 cm (Visser *et al.*, 2010; Bock *et al.*, 2011b) and are based on undifferenced GPS observations processed with the Bernese GPS software package (Dach *et al.*, 2007). Kinematic orbits may contain data gaps since positions can be estimated only at epochs for which a sufficient number of GPS satellites is visible. PSO availability over the considered period is shown in more detail in Table 2.

Precise GPS orbits, delivered with a 15 min sample interval and 30 s clock solutions were obtained from IGS Final Products ftp website (IGS, 2013b) for each day of each GPS week. The accuracy is about 2.5 cm for GPS orbits and about 75 ps for clock solutions and is reported on the IGS Products website (IGS, 2013a).

GOCE orbits are estimated with respect to the centre of mass (CoM) of the satellite, so

Table 2 - GOCE PSO availability: daily reports over the period November 1, 2009 - May 31, 2011.

PSO

2009	1	2	3	4	5	6	7	8	9	10	11	12	13	14	15	16	17	18	19	20	21	22	23	24	25	26	27	28	29	30	31
November	305	306	307	308	309	310	311	312	313	314	315	316	317	318	319	320	321	322	323	324	325	326	327	328	329	330	331	332	333	334	
December	335	336	337	338	339	340	341	342	343	344	345	346	347	348	349	350	351	352	353	354	355	356	357	358	359	360	361	362	363	364	365
2010																															
January	1	2	3	4	5	6	7	8	9	10	11	12	13	14	15	16	17	18	19	20	21	22	23	24	25	26	27	28	29	30	31
February	32	33	34	35	36	37	38	39	40	41	42	43	44	45	46	47	48	49	50	51	52	53	54	55	56	57	58	59			
March	60	61	62	63	64	65	66	67	68	69	70	71	72	73	74	75	76	77	78	79	80	81	82	83	84	85	86	87	88	89	90
April	91	92	93	94	95	96	97	98	99	100	101	102	103	104	105	106	107	108	109	110	111	112	113	114	115	116	117	118	119	120	
May	121	122	123	124	125	126	127	128	129	130	131	132	133	134	135	136	137	138	139	140	141	142	143	144	145	146	147	148	149	150	151
June	152	153	154	155	156	157	158	159	160	161	162	163	164	165	166	167	168	169	170	171	172	173	174	175	176	177	178	179	180	181	
July	182	183	184	185	186	187	188	189	190	191	192	193	194	195	196	197	198	199	200	201	202	203	204	205	206	207	208	209	210	211	212
August	213	214	215	216	217	218	219	220	221	222	223	224	225	226	227	228	229	230	231	232	233	234	235	236	237	238	239	240	241	242	243
September	244	245	246	247	248	249	250	251	252	253	254	255	256	257	258	259	260	261	262	263	264	265	266	267	268	269	270	271	272	273	
October	274	275	276	277	278	279	280	281	282	283	284	285	286	287	288	289	290	291	292	293	294	295	296	297	298	299	300	301	302	303	304
November	305	306	307	308	309	310	311	312	313	314	315	316	317	318	319	320	321	322	323	324	325	326	327	328	329	330	331	332	333	334	
December	335	336	337	338	339	340	341	342	343	344	345	346	347	348	349	350	351	352	353	354	355	356	357	358	359	360	361	362	363	364	365
2011																															
January	1	2	3	4	5	6	7	8	9	10	11	12	13	14	15	16	17	18	19	20	21	22	23	24	25	26	27	28	29	30	31
February	32	33	34	35	36	37	38	39	40	41	42	43	44	45	46	47	48	49	50	51	52	53	54	55	56	57	58	59			
March	60	61	62	63	64	65	66	67	68	69	70	71	72	73	74	75	76	77	78	79	80	81	82	83	84	85	86	87	88	89	90
April	91	92	93	94	95	96	97	98	99	100	101	102	103	104	105	106	107	108	109	110	111	112	113	114	115	116	117	118	119	120	
May	121	122	123	124	125	126	127	128	129	130	131	132	133	134	135	136	137	138	139	140	141	142	143	144	145	146	147	148	149	150	151

LEGEND

Available and converted
Not available

modeling GPS observations requires precise coordinates of the centre of the mounting plane (CMP) of the main GOCE GPS antenna (SSTI-A) with respect to the satellite CoM. Table 3 shows coordinates of the GOCE CoM and SSTI-A antenna CMP in the Satellite Reference Frame (SRF). No change in the CoM location has been modelled, keeping its coordinates constant and equal to the Beginning Of Life (BOL) conditions. Fig. 1 shows a schematic view of the GOCE satellite, with the location of the two SSTI antennas and the layout of the right-handed SRF and the SSTI-A Antenna Reference Frame (ARF).

Table 3 - Coordinates of the satellite CoM and SSTI-A antenna CMP in the SRF (Bigazzi and Frommknecht, 2010).

	X_{SRF} (m)	Y_{SRF} (m)	Z_{SRF} (m)
CoM	2.5000	0.0036	0.0011
CMP	3.1930	0.0000	-1.0922

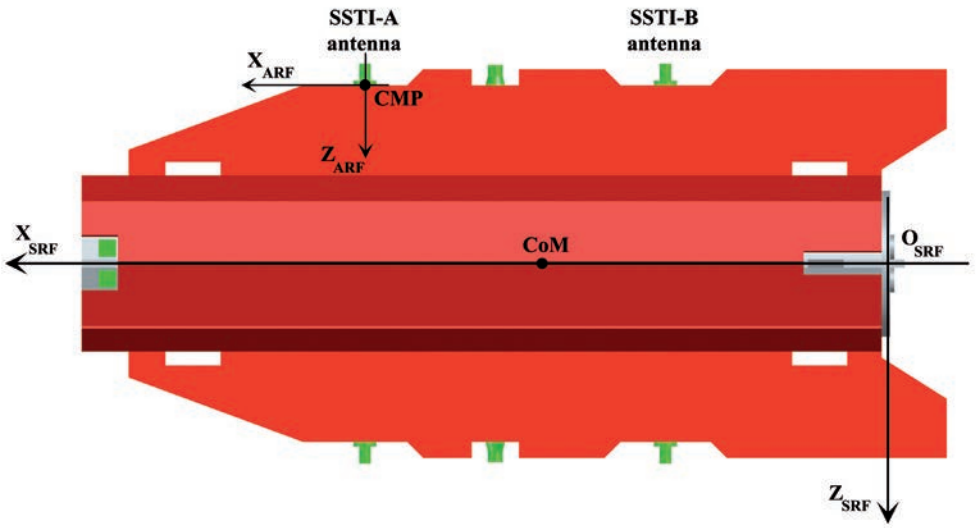

Fig. 1 - Schematic view of the SSTI antenna locations and the SRF and ARF reference systems.

Moreover, because the antenna phase centre location differs from the CMP, it is necessary to determine two sets of phase centre corrections: Phase Centre Offsets (PCOs), defining the position of the mean antenna phase centre with respect to the CMP (Table 4), and Phase Centre Variations (PCVs), accounting for the azimuth and zenith/nadir dependence, which are both provided in ANTEX (ANTenna EXchange) format for the L1 and L2 frequencies in an antenna-fixed reference frame and are available on the GOCE SSTI-A ANTEX website (GOCE SSTI-A ANTEX, 2013). The impact of PCVs on the POD process is important, reaching magnitude up to 3 - 4 cm. In fact, while PCO vectors are fixed, PCVs were estimated from in-flight calibration using 154 days of GOCE GPS data (Bock *et al.*, 2011a). In general, both PCOs and PCVs are sources of significant systematic errors in GPS data processing if not correctly modeled (Jäggi *et al.*, 2009).

Other auxiliary parameters for GOCE POD processing were retrieved from the European Space Operations Centre (ESA/ESOC) ftp website (ESA/ESOC, 2013), in particular a GOCE radiation area of 11.2 m^2, a drag area of 1.035 m^2, and Euler angles describing a 3-2-1 rotation from the SRF to the ARF (see Table 5). A constant satellite mass of 1050 kg was used. According to Drinkwater *et al*. (2007) the yaw-steering mode was used for the attitude modeling.

Table 4 - SSTI-A antenna PCOs in the ARF for both frequencies L1 and L2 (Bock *et al*., 2011a).

X_{ARF} (mm)	Y_{ARF}(mm)	Z_{ARF} (mm)
L1 -0.18	3.51	-81.11
L2 -1.22	-1.00	-84.18

Table 5 - Euler rotation angles from the SRF to the ARF (ESA/ESOC, 2013).

	X_{SRF} Axis (deg)	Y_{SRF} Axis (deg)	Z_{SRF} Axis (deg)
Euler Rotation Angle	180.0	0.0	90.0

3. Dynamical model

The Earth's static gravity field used in the GOCE POD processing is the EIGEN-6C model (Förste *et al*., 2011) up to degree and order 200, combining LAGEOS, GRACE and GOCE satellite measurements, gravity and altimetric data, available from the International Centre for Global Earth Models (ICGEM) website (ICGEM, 2013).

The third-body gravitational forces of the Sun, the Moon and the planets are considered, together with the indirect oblateness perturbation, which is a feedback effect originating from the interaction of the lunar motion perturbed by the Earth second zonal harmonic.

Solid Earth and ocean tide perturbations are included in the dynamical model. Earth tides are modeled according to the IERS-TN32 solid tide model (McCarthy and Petit, 2003), while the FES2004 model (Lyard *et al*., 2006) up to degree and order 50 for 106 constituents has been adopted for ocean tides.

The satellite acceleration is also corrected for general relativistic effects due to the curvature of space-time generated by a rotating Earth (McCarthy and Petit, 2003).

Three analytical models are implemented in NAvigation Package for Earth Observation Satellites (NAPEOS) in order to compute the non-gravitational perturbations due to Solar Radiation Pressure (SRP) (McCarthy and Petit, 2003), Earth albedo and infrared radiation (Arnold and Dow, 1984). In particular, SRP coefficients are estimated during the POD process considering a constant GOCE radiation cross-section area, while the albedo and infrared coefficients are fixed.

The aerodynamic forces are not considered during the POD process because GOCE is flying in a quasi drag-free mode via an electric propulsion system used to continuously counteract the atmospheric drag in the direction of the motion.

Finally, empirical accelerations in the radial (r), along-track (a) and cross-track (c) directions can be included in the force model to compensate model omission errors. They consist of a combination of two periodic terms, each a function of the satellite argument of latitude u, and a constant one, as follows:

$$\Delta \vec{a}_r = (a_{r0} + a_{rc} \cos u + a_{rs} \sin u)\, \vec{u}_r$$

$$\Delta \vec{a}_a = (a_{a0} + a_{ac} \cos u + a_{as} \sin u)\, \vec{u}_a \qquad (1)$$

$$\Delta \vec{a}_c = (a_{c0} + a_{cc} \cos u + a_{cs} \sin u)\, \vec{u}_c.$$

The nine parameters appearing in these equations are referred to as CPRs because the period of these accelerations is one cycle per revolution. The three radial CPRs are not considered in the adopted force model because there is a direct correlation between these and along-track CPRs. Thus, only the along-track and cross-track parameters are estimated over hourly intervals, which establishes a densely-parameterized, fully dynamic POD approach.

Tables 6 and 7, respectively, exhibit the force models and the estimated and fixed parameters adopted for the GOCE POD process.

Table 6 - Gravitational, non-gravitational and empirical forces adopted for the GOCE POD process.

Dynamical models	Description	Reference
Static gravity field	EIGEN-6C 200x200	(a)
Solid Earth tides	IERS-TN32	(b)
Ocean tides	FES2004 106 constituents, 50x50	(c)
Third body perturbation	Lunar gravity Solar gravity Planetary gravity Indirect oblateness perturbation	
Relativistic correction	Correction according to general relativity	(b)
Aerodynamic forces	not considered	
Radiation Pressure	Solar radiation pressure Albedo radiation pressure Infrared radiation pressure	(b) (d) (d)
Empirical accelerations	CPR along-, cross-track parameters	(e)

(a) Förste *et al.* (2011); (b) McCarthy and Petit (2003); (c) Lyard *et al.* (2006); (d) Arnold and Dow (1984); (e) ESA/ESOC (2009).

Table 7 - Estimated and fixed parameters during the GOCE POD process.

Parameters	Description	Type	Reference
State vector		estimated	
Radiation pressure	Solar radiation pressure Albedo radiation pressure Infrared radiation pressure	estimated fixed, equal to 1 fixed, equal to 1	(a) (b) (b)
Empirical accelerations	CPR constant along-track CPR constant cross- track CPR cosine along- track CPR cosine cross- track CPR sine along- track CPR sine cross- track	estimated (1 per hour) estimated (1 per hour) estimated (1 per hour) estimated (1 per hour) estimated (1 per hour) estimated (1 per hour)	(c) (c) (c) (c) (c) (c)

(a) McCarthy and Petit (2003); (b) Arnold and Dow (1984); (c) ESA/ESOC (2009).

4. Fully dynamic orbit generation

NAPEOS, developed and maintained by ESA, was used to perform the GOCE POD. This software system is composed of several *programs* that perform different tasks. A POD task is implemented through a script, which is used to set up a *sequence* which calls different programs and organizes the I/O channels between them under specific processing procedures, called *modes*. Three sequences were defined to process GOCE data (see Fig. 2). They are described in the following, and where appropriate the specific program and its mode is provided in the form *Program*/*Modes*. The POD products contain the GPS observation residuals, the estimated parameters and the estimation covariance matrices.

4.1. The sequence GOCE_PSO_a

The sequence starts with the IGS clock files that are converted to NAPEOS clock files format (.tcb) for the 24 h of the analyzed day (*ClockUpd*/*GOCE*). The satellite positions from the PSO orbits are converted to NAPEOS Tracking Data Format (NTDF) (*Tracksim*/*ORBIT-FIT*) that are then used to generate the best-fitting orbit for the day being processed (*Bahn*/*ORBIT-FIT*). As a result ofthis step the parameters shown in Table 7 are estimated and an a-priori orbit is generated. The IGS sp3 orbits are merged with the computed a-priori orbit to obtain a combined sp3 (*OrbUpd*/*ORBIT-FIT*). The RINEX files available for the day being processed are collected in a catalogue file (*BuildCat*/*GOCE*), and pre-processed to initialize the receiver clocks are estimated at the same time (*GnssObs*/*GOCE-RAW*). A first raw orbit is then computed at metre level using only GPS undifferenced pseudorange observations, and GOCE clocks (*Bahn*/*GOCE-RAW*). In this step the pre-computed satellite state vector, C_R and CPRs are used to initialize the estimation process. The resulting raw orbit is then merged with the IGS sp3 orbits (*OrbUpd*/*GOCE-RAW*). The available observations are then pre-processed (*GnssObs*/*GOCE*) and the effective orbit estimation is performed at millimetre level using both the GPS undifferenced carrier phase and pseudorange observations, taking as input the a-priori raw orbit and the initialized parameters and clocks (*Bahn*/*GOCE*).

4.2. The sequence GOCE_PSO_b

It was observed that *GnssObs* was not utilizing all the available observations for some daily arcs. This was traced to a large disalignment of the observation time tag with respect to an integer second. The problem was fixed by tweaking steps *GnssObs*/*GOCE-RAW* and *GnssObs*/*GOCE* of sequence GOCE_PSO_a to instruct the program to correct both measurements and time tags to bring the measurement to an integer second, and by setting the interval between observations, for them to be considered simultaneous, to 1.0 and 0.9 s respectively for the *GnssObs GOCE-RAW* and *GOCE* modes.

4.3. The sequence GOCE_c

This sequence is identical to the GOCE_PSO_a sequence, except that it uses as the a-priori orbit the one propagated from the previous day rather than the PSO solution. This was necessary due to the lack of convergence of the POD task based on the kinematic PSO solutions. This behavior is probably due to the presence of gaps in the kinematic PSO ephemeris, but warrants further investigation.

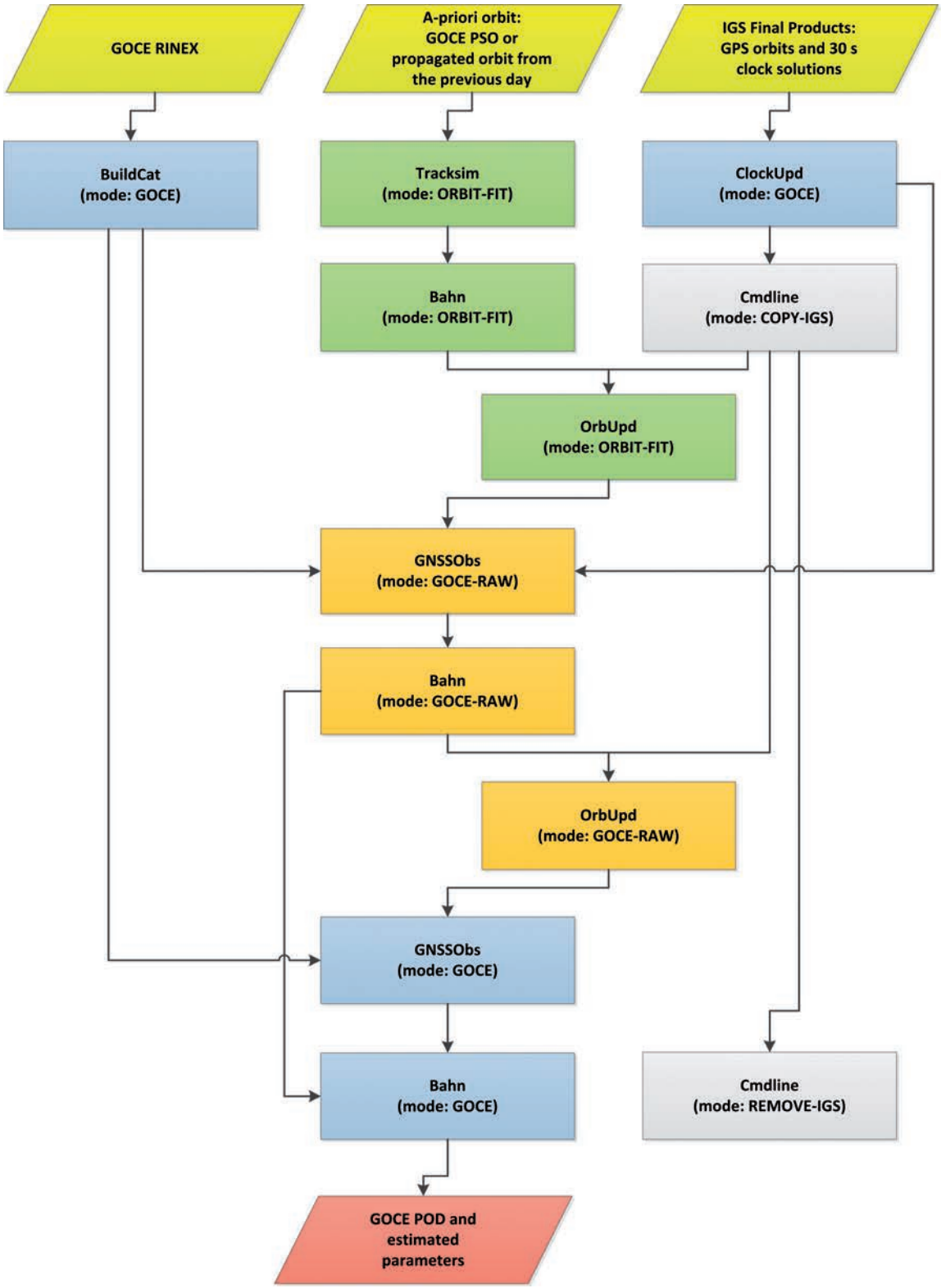

Fig. 2 - General sequence of NAPEOS programs used for GOCE POD process.

5. POD results

The three sequences described in Section 4 were executed for each 24-hour observation period to cover all GOCE data available from November 1, 2009 to May 31, 2011 for a total of 496 days. The GOCE_PSO_a sequence was applied in the first place, then the GOCE_PSO_b sequence was selectively applied to those days where GOCE_PSO_a sequence failed to converge, or where the resulting post-fit RMS was greater than 1 cm. The GOCE_c sequence, which is based on the orbit propagated from the previous day's solution, was run for those days where the PSO was not available, or where the previous sequences had failed or given inaccurate results. The statistics of successful processing for the different sequences are shown in Table 8. A comprehensive view of the data availability, post-fit RMS level, and the successful sequence applied on each of the 496 days of the data interval considered is shown in Table 8. The three sequences were successfully run for 487 days of the total available days of data (98.2%) and the POD task was performed with a RMS below 10 mm for 448 days (90.3%).

Table 8 - Statistics of the GOCE POD process for the three sequences.

Run sequences	Days successfully processed	Days with *RMS* ≤ 1 cm	Percentage of days processed	Percentage of days *RMS* ≤ 1 cm
GOCE _PSO_a	375	339	75.6	68.3
GOCE _PSO_a,_b	426	377	85.9	76.0
GOCE_PSO_a,_b,_c	487	448	98.2	90.3

As Table 8 shows, the POD was carried out with lower accuracy (a value of the RMS greater than 10 mm) for the periods immediately after the data gaps (i.e., February and September 2010) and several days in 2011. For the majority of the daily data available for 2011, the sequences based on the PSO orbits failed due to divergence in the estimation process. The third sequence was hence run, and this allowed to perform the POD successfully for the majority of the missing days. In Fig. 3 (in blue), where the daily RMS of the residuals for the undifferenced carrier phase are reported, it is possible to observe that most of the results exhibit value between 6.7 mm and 6.8 mm, and that only a few spikes exceed the 1.5 cm level.

Fig. 4 shows the total number of observations available for *Bahn* processing for each day of data. The average number of observations is about 28000 per day, while the average of the rejected observations is about 515 per day. For the majority of the days processed the number of rejected observations is below 300 (about 1% of the total available observations), but for some days (i.e., Day Of Year (DOY) 295, 296, 297, 310, 314, 315, 318 of year 2010) the number of rejections is much higher (even more than 50% of the observations are sometimes rejected). For those days where a huge number of observations was rejected, the flag that corrects measurements and time tags to bring the measurements to the integer second was set in the data pre-processing program (*GnssObs*). This flag allowed to utilize all the available observations but, in turn, sometimes reduced the accuracy of the estimated orbits leading to a high observation rejection rate.

Table 9 - Statistics of GOCE POD processing over the period from November 1, 2009 to May 31, 2011.

POD results

2009	1	2	3	4	5	6	7	8	9	10	11	12	13	14	15	16	17	18	19	20	21	22	23	24	25	26	27	28	29	30	31
November	305	306	307	308	309	310	311	312	313	314	315	316	317	318	319	320	321	322	323	324	325	326	327	328	329	330	331	332	333	334	
December	335	336	337	338	339	340	341	342	343	344	345	346	347	348	349	350	351	352	353	354	355	356	357	358	359	360	361	362	363	364	365
2010																															
January	1	2	3	4	5	6	7	8	9	10	11	12	13	14	15	16	17	18	19	20	21	22	23	24	25	26	27	28	29	30	31
February	32	33	34	35	36	37	38	39	40	41	42	43	44	45	46	47	48	49	50	51	52	53	54	55	56	57	58	59			
March	60	61	62	63	64	65	66	67	68	69	70	71	72	73	74	75	76	77	78	79	80	81	82	83	84	85	86	87	88	89	90
April	91	92	93	94	95	96	97	98	99	100	101	102	103	104	105	106	107	108	109	110	111	112	113	114	115	116	117	118	119	120	
May	121	122	123	124	125	126	127	128	129	130	131	132	133	134	135	136	137	138	139	140	141	142	143	144	145	146	147	148	149	150	151
June	152	153	154	155	156	157	158	159	160	161	162	163	164	165	166	167	168	169	170	171	172	173	174	175	176	177	178	179	180	181	
July	182	183	184	185	186	187	188	189	190	191	192	193	194	195	196	197	198	199	200	201	202	203	204	205	206	207	208	209	210	211	212
August	213	214	215	216	217	218	219	220	221	222	223	224	225	226	227	228	229	230	231	232	233	234	235	236	237	238	239	240	241	242	243
September	244	245	246	247	248	249	250	251	252	253	254	255	256	257	258	259	260	261	262	263	264	265	266	267	268	269	270	271	272	273	
October	274	275	276	277	278	279	280	281	282	283	284	285	286	287	288	289	290	291	292	293	294	295	296	297	298	299	300	301	302	303	304
November	305	306	307	308	309	310	311	312	313	314	315	316	317	318	319	320	321	322	323	324	325	326	327	328	329	330	331	332	333	334	
December	335	336	337	338	339	340	341	342	343	344	345	346	347	348	349	350	351	352	353	354	355	356	357	358	359	360	361	362	363	364	365
2011																															
January	1	2	3	4	5	6	7	8	9	10	11	12	13	14	15	16	17	18	19	20	21	22	23	24	25	26	27	28	29	30	31
February	32	33	34	35	36	37	38	39	40	41	42	43	44	45	46	47	48	49	50	51	52	53	54	55	56	57	58	59			
March	60	61	62	63	64	65	66	67	68	69	70	71	72	73	74	75	76	77	78	79	80	81	82	83	84	85	86	87	88	89	90
April	91	92	93	94	95	96	97	98	99	100	101	102	103	104	105	106	107	108	109	110	111	112	113	114	115	116	117	118	119	120	
May	121	122	123	124	125	126	127	128	129	130	131	132	133	134	135	136	137	138	139	140	141	142	143	144	145	146	147	148	149	150	151

STATISTICS	
Days TOT	496
Days not done	9
Days done	487
POD with RMS > 1 cm	39
POD with RMS < 1 cm	448
% of performed POD	98.2
% of POD with RMS < 1cm	90.3

LEGEND
POD with RMS <= 1 cm
POD with RMS > 1 cm
POD not performed
Missing Data

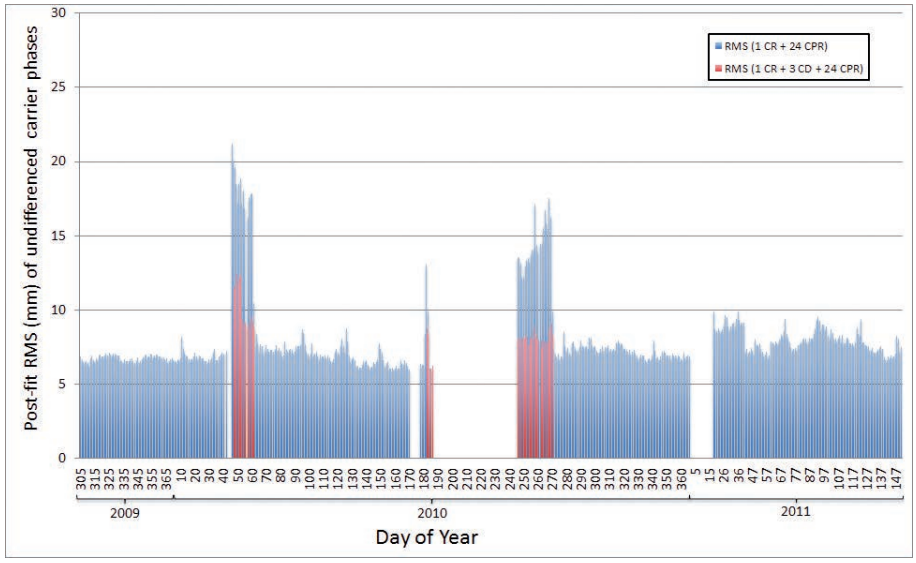

Fig. 3 - Post-fit RMS of undifferenced carrier phases (in millimetres) for the data processed. Drag-free arcs (no C_D estimated) are shown in blue, non-drag-free arcs (C_D estimated) are shown in red.

The parameters thus estimated were then analyzed. The solar radiation coefficient C_R, estimated daily, is shown (in blue) in Fig. 5 with a large scatter of 3.97 about a mean value of 2.48. This behavior points to some deficiencies in our modeling, since negative values also appear and some form of signal seems to be present, notwithstanding the discontinuities due to data outages. The hourly estimated CPRs for the along-track and cross-track components

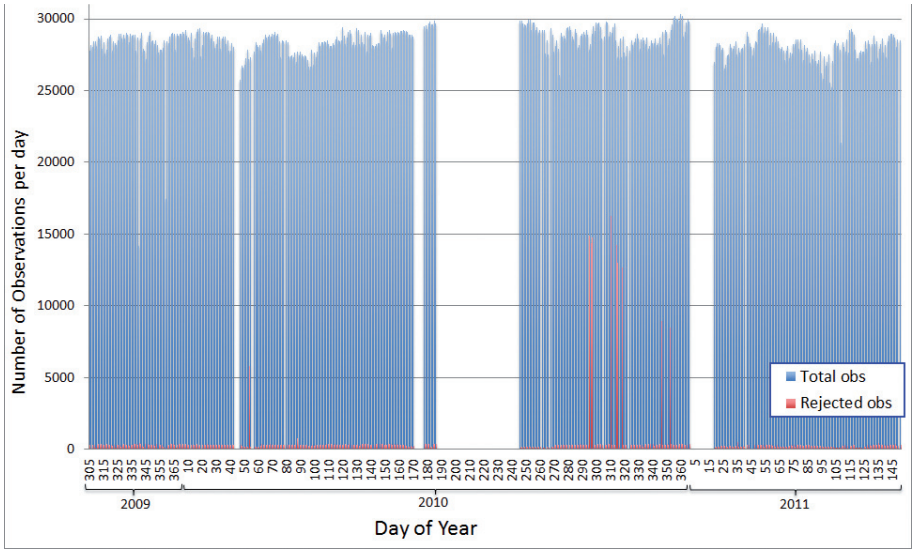

Fig. 4 - Number of undifferenced carrier phase observations processed (blue) or rejected (red) each day from November 1, 2009 to May 31, 2011.

are respectively shown in blue in Figs. 6 and 7. The CPR values are generally constant, except for large variations of 2 orders of magnitude (from about 10^{-11} to 10^{-09} km/s^2) in the along-track component near the data gaps of February, July and September, 2010. The same effect is also observed, but to a lesser extent, in the cross-track CPRs. No C_R or CPR coefficients are plotted from DOY 19 to 40 of 2011, because they are associated with an unmodeled switch of the GOCE GPS antenna, as explained later.

The unexpected pattern of the non-gravitational parameters solution prompted us to investigate whether the satellite had suffered any anomalous behavior near those dates. It was found (ESA, 2012a, 2012b, 2012c) that in February, July and September, 2010 GOCE had no longer been orbiting in the nominal drag-free mode, since the ion thruster had been biased in order to raise the orbit for altitude recovery following spacecraft anomalies. Clearly, the estimation of the along-track CPR coefficients is not capable of accurately modeling the satellite thrust, as shown by the associated higher post-fit RMS values shown in blue in Fig. 3.

The change in the satellite dynamics due to the action of the ion thruster was then introduced in the NAPEOS force model through the activation of the atmospheric drag model. Precise orbit determination runs were performed only for the days where drag-free mode was not operating. Three piecewise-linear drag coefficients (C_Ds) per arc were estimated, one every 12 hours. Their values are shown in Fig. 8 and are mostly - and paradoxically - positive, ranging between 3 and 5. The resulting post-fit RMS, shown in red in Fig. 3, is significantly reduced with respect to the previously used force model, where no C_Ds were estimated. The computed RMS is generally below 10 mm, except for a few days during February, 2010. The newly estimated values for the solar radiation pressure coefficients and for the along- and cross-track CPRs are shown respectively in red in Figs. 5, 6 and 7. While the behavior of the newly estimated values of the C_Ds is not so different from that of the previously estimated values, the CPRs - mainly the along-track component, show a smaller excursion, except for the constant term over a few days in February, 2010.

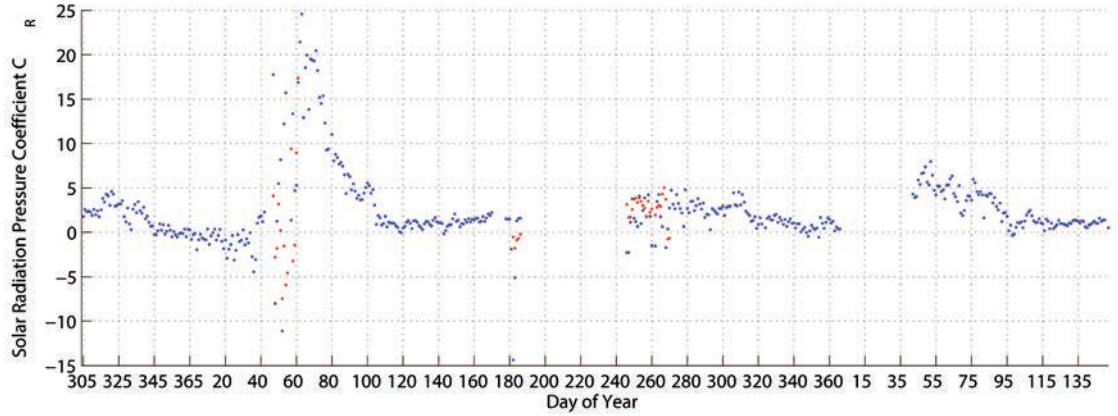

Fig. 5 - Behaviour of the solar radiation pressure coefficients C_Rs, estimated once per day. Drag-free arcs (no C_D estimated) are shown in blue, non-drag-free arcs (C_D estimated) are shown in red (DOY starts in 2009).

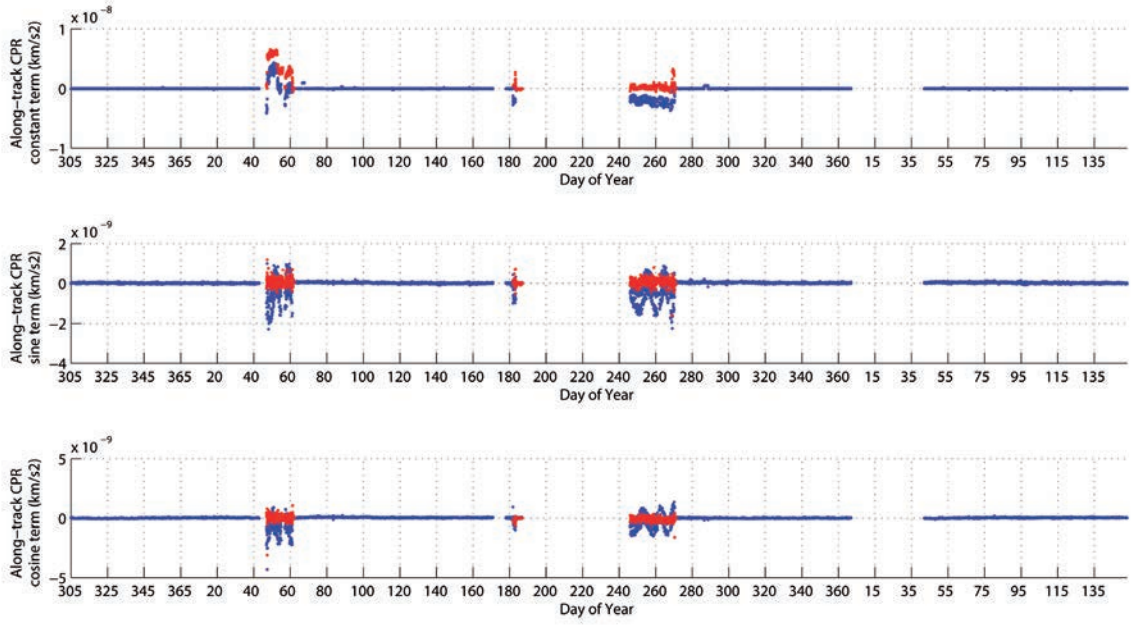

Fig. 6 - Behaviour of the hourly estimated constant, sine and cosine components of the along-track CPR coefficients. Drag-free arcs (no C_D estimated) are shown in blue, non-drag-free arcs (C_D estimated) are shown in red (DOY starts in 2009).

The precise orbits determined using NAPEOS were then compared with the official kinematic and reduced-dynamics PSOs for all the available days of data. The comparison is shown in Fig. 9 for the kinematic PSOs and Fig. 10 for the reduced-dynamics PSOs. The 3D RMS - later referred to as the *distance* between orbits - is below 10 cm for most of the orbit comparisons (76% and 83% of the total available days of data, respectively, for the kinematic and reduced-dynamics PSOs). Before DOY 200 of 2010 both the POD RMS and the POD-PSO

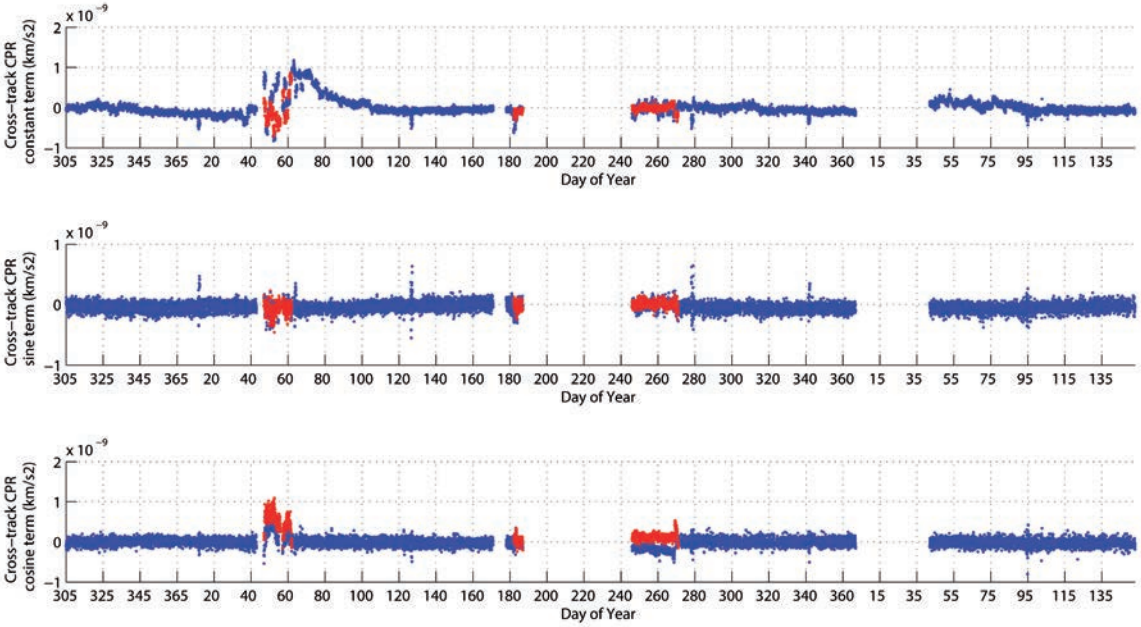

Fig. 7 - Behaviour of the hourly estimated constant, sine and cosine components of the cross-track CPR coefficients. Drag-free arcs (no C_D estimated) are shown in blue, non-drag-free arcs (C_D estimated) are shown in red (DOY starts in 2009).

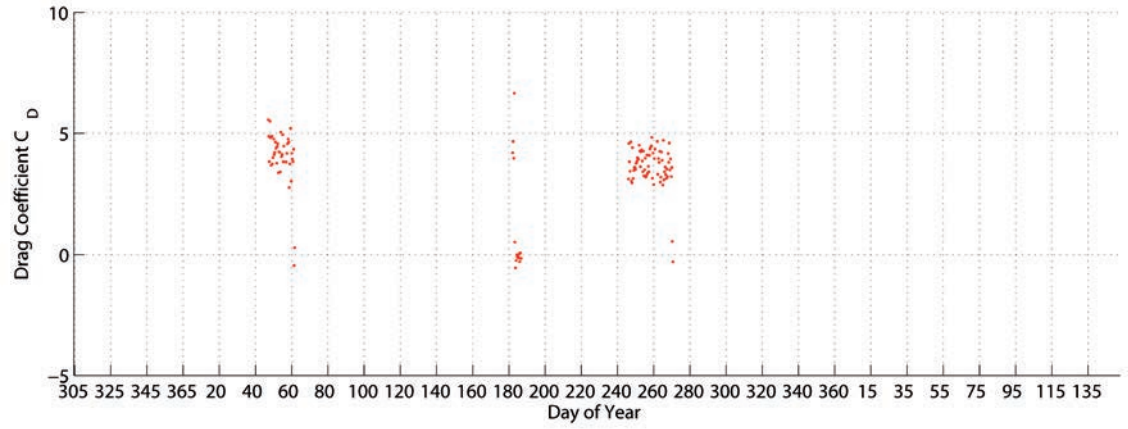

Fig. 8 - Behaviour of the piecewise-linear drag coefficients C_Ds, estimated once per day over the period of non-drag-free motion (DOY starts in 2009).

orbit distance are generally low, while after DOY 240 of 2010, the RMSs have higher values, especially during 2011.

There is a high degree of correlation between days showing a post-fit RMS higher than 3 cm and the RMS of the distance of the resulting ephemeris from the PSO orbits. Among the orbits estimated with a post-fit RMS less than 10 mm, about 40% and 20% significantly (3D RMS > 6 cm) differ respectively from the kinematic and reduced-dynamics PSO solutions, sometimes

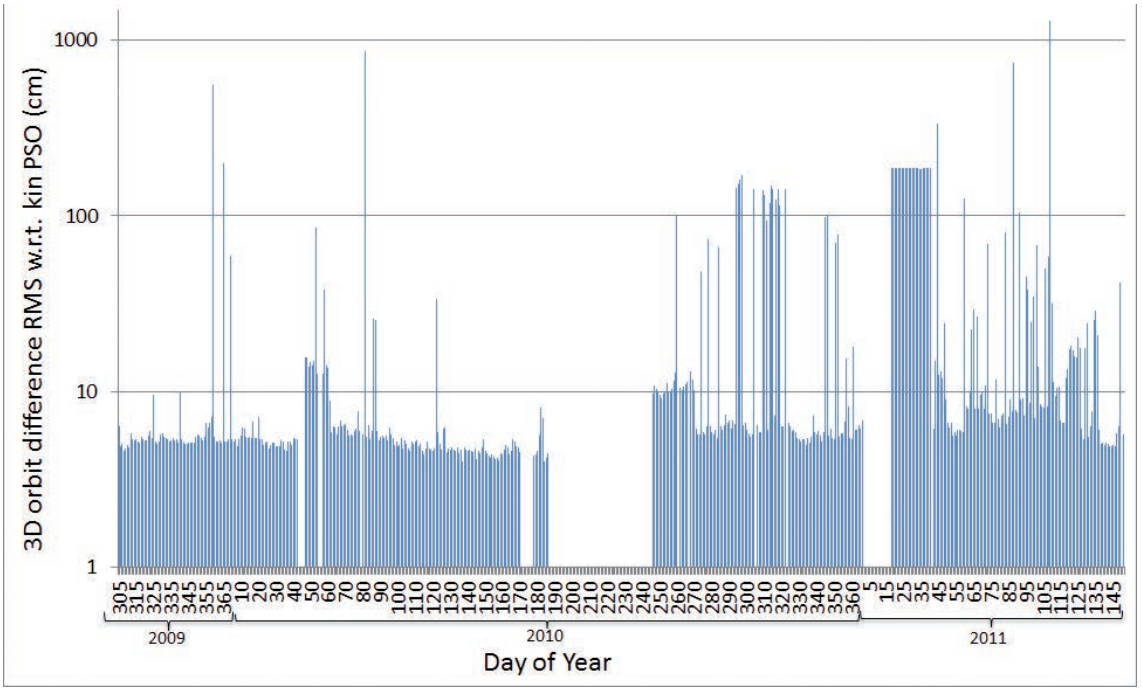

Fig. 9 - Comparison between the estimated and the official kinematic PSO orbits in the Earth-Centred Earth-Fixed (ECEF) reference frame. The 3D orbit difference RMS with respect to the kinematic PSOs is shown in centimetres.

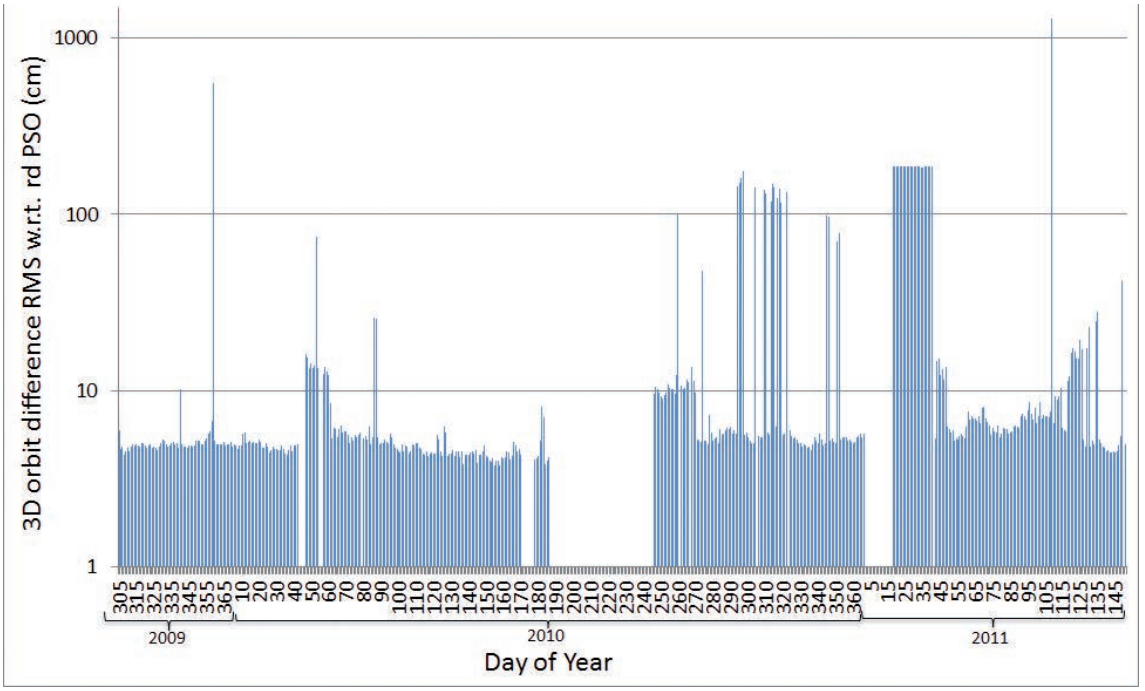

Fig. 10 - Comparison between the estimated and the official reduced-dynamics PSO orbits in the Earth-Centred Earth-Fixed (ECEF) reference frame. The 3D orbit difference RMS with respect to the reduced-dynamics PSOs is shown in centimetres.

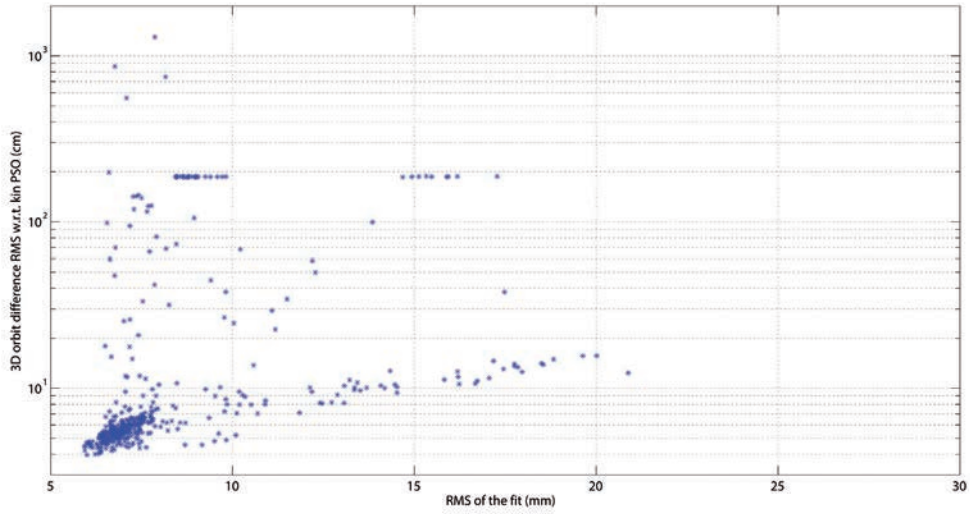

Fig. 11 - Comparison between the estimated and the official kinematic PSO orbits. The 3D orbit difference RMS with respect to the kinematic PSO's is plotted against the post-fit RMS.

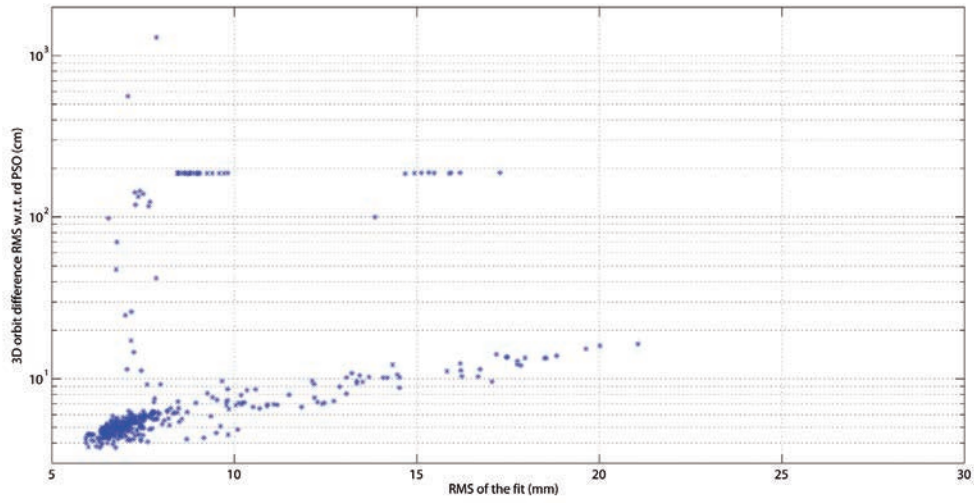

Fig. 12 - Comparison between the estimated and the official reduced-dynamics PSO orbits. The 3D orbit difference RMS with respect to the reduced-dynamics PSOs is plotted against the post-fit RMS, showing a linear correlation.

reaching a position difference RMS up to several metres. Some of these arcs are characterized by not all the observations being used in the GOCE POD process, thus leading to low accuracy orbits even if a low value of the residuals RMS was achieved.

The correlation between the RMS of the residuals of the estimated orbits and the 3D RMS of the difference between these orbits and the PSO orbits is more evident in both Figs. 11 and 12. The majority of the data analyzed (about 70% and 75% of the orbits compared, respectively with the kinematic and reduced-dynamics PSO solutions) is located at the lower left corner

of the plot, where the RMS of the fit is below 10 mm and the 3D RMS is lower than 10 cm. Increasing values of the post-fit RMS correspond to higher values of the POD-PSO 3D RMS. These data are distributed linearly on the semi-log plot. The POD-PSO 3D RMS is between 10 cm and 12 m even if the POD RMS is below 10 mm for about 60 and 40 days of data respectively compared with the kinematic and reduced-dynamics PSO solutions. This is partly due to sparseness of the observations used and partly to the unmodeled switch of the GPS antenna for the period immediately after the SSTI anomaly occurred on January 2, 2011 (ESA, 2011a, 2011b). During the period between January 2, 2011 and February 10, 2011 the redundant GPS antenna (SSTI-B) was used to track the satellite, but this was not taken into account in the NAPEOS processing scheme. This is clearly observable in Figs. 9 and 10, where the POD-PSO 3D RMS shows an almost constant bias of about 186 cm (the distance between SSTI-A and SSTI-B is about 183 cm), as well as in Fig. 3, which shows an anomalously high and constant post-ft RMS for these dates, and in Figs. 11 and 12, where two flat series of constant orbit distance values appear independent of the value of the post-fit RMS.

In order to evaluate the internal quality of the POD results, the regular 24-hour arc length used for orbit determination was extended for 366 arcs to 30 hours, thus ensuring 6-hour overlaps centred at 24:00 each day. To avoid boundary effects, the comparison of the overlaps was carried out considering only the central 5 hours (21:30 - 02:30). This showed an average distance of the overlapping arcs of 9.6 mm.

6. Conclusions

The precise orbit determination of GOCE was successfully carried out for a total of 487 daily arcs over the period from November 1, 2009 to May 31, 2011, which includes all tracking measurements from the LAGRANGE GPS receiver onboard GOCE which were publicly available at the time of processing. The NAPEOS software system was used to carry out the orbit determination task. Results show an average post-fit RMS of the undifferenced GPS carrier phase observations below 10 mm for 448 days, or 90.3% of the total. This may be partly due to degraded system performance immediately after loss of telemetry (February 12 - 14, 2010) and onboard computer failures (July - August, 2010).

The quality of the POD results obtained using NAPEOS was evaluated internally by computing the difference between 5 hour-long overlapping arcs, which shows an average RMS of 9.6 mm. An external evaluation of the quality was obtained by comparing our orbits with the official project kinematic and reduced-dynamics PSO orbits over the entire data span. Note that there is a fundamental difference between the orbit reduction approaches used for determining the kinematic PSOs and the orbits estimated here. The approach adopted by the GOCE-Italy team is a densely-parameterized, fully dynamical method, while the official kinematic PSO orbits are computed based on a kinematical approach, which is subject to leaving wide gaps in the reconstructed ephemeris due to its lack of capability to predict and interpolate orbital arcs. The 3D RMS difference between the orbits determined in this investigation and the official PSO solutions is below 10 cm for about 70% and 75% of the daily arcs when compared, respectively, with the kinematic and reduced-dynamics versions. In particular, days with a post-fit RMS higher than 3 cm also exhibit a fairly high RMS of the distance from both kinematic

and reduced-dynamics PSO orbits. Among the orbits estimated with a good post-fit RMS (RMS < 10 mm), about 30% and 15% respectively differ (3D RMS > 6 cm) from the kinematic and reduced-dynamics PSO solutions, sometimes reaching a position difference RMS up to several metres. This result is mainly caused by sparseness in the observations available for processing and to a non-modeled switch of the GPS receiver antenna.

The results obtained are encouraging, but further investigation is needed to overcome several weak points in the analysis. In particular, the next phase of the investigation will make use of the thrust history profile as well as of the attitude and mass history profiles. Together these additions will contribute to improving the force modeling in such a way as to resolve the paradoxical result of positive drag coefficients during the orbit raising phase and explain the apparent signal in the radiation pressure coefficient time series. The orbital fit will also improve due to correct modeling of the GPS antenna in use.

The present results, and the expected improvement from the next study phase, form a solid basis for an investigation of the recovery of ocean tide parameters which is being carried out as a parallel task. In fact, both PSO orbit types can absorb tidal perturbation signal that the NAPEOS force model, however densely parameterized, cannot. Besides, the partials with respect to the tidal parameters are not available from the official GOCE products. Thanks to its low altitude of about 250 km, GOCE is well suited to tidal recovery, except for aliasing problems stemming from Sun-synchronicity, through the application of classical orbit perturbation analysis methods. This requires an extension of the NAPEOS solution capability to include ocean tide parameters, which has recently been implemented (Bardella and Casotto, 2012).

Acknowledgements. The authors gratefully acknowledge the GOCE-Italy project funded by the ASI. We thank H. Bock and F. Vespe for their critical review of the manuscript. A special thank goes to T. Springer and his group for NAPEOS software support. The ESA is also acknowledged for providing the GOCE data.

REFERENCES

Arnold S.J. and Dow J.M.; 1984: *Models for spacecraft acceleration due to earth albedo and infrared radiation*. OAD WP n. 265.

Bardella M. and Casotto S.; 2012: *Extending ESA's NAPEOS S/W system for ocean tide parameter recovery*. In: Proc. 23rd Int. Symp. Space Flight Dyn., Pasadena, CA, U.S.A., pp. 1-16, https://issfd.jpl.nasa.gov/home/assets/papers/ISSFD23_PS_13.pdf.

Bigazzi A. and Frommknecht B.; 2010: *Note on GOCE instruments positioning*. European Space Agency, Issue 3.1, XGCE-GSEG-EOPG-TN-09-0007.

Bock H., Jäggi A., Meyer U., Dach R. and Beutler G.; 2011a: *Impact of GPS antenna phase center variations on precise orbits of the GOCE satellite*. Adv. Space Res., **47**, 1885-1893, doi:10.1016/j.asr.2011.01.017.

Bock H., Jäggi A., Meyer U., Visser P.N.A.M., van den Ijssel J., van Helleputte T., Heinze M. and Hugentobler U.; 2011b: *GPS-derived orbits for the GOCE satellite*. J. Geod., **85**, 807-818, doi:10.1007/s00190-011-0484-9.

Bock H., Jäggi A., Svehla D., Beutler G., Hugentobler U. and Visser P.N.A.M.; 2007: *Precise orbit determination for the GOCE satellite using GPS*. Adv. Space Res., **39**, 1638-1647, doi:10.1016/j.asr.2007.02.053.

Dach R., Hugentobler U., Fridez P. and Meindl M. (eds); 2007: *Bernese GPS Software Version 5.0*, *user manual*. Astronomical Institute, University of Bern, Bern, Switzerland, http://www.bernese.unibe.ch/docs50/DOCU50.pdfhttp://www.bernese.unibe.ch/docs50/DOCU50.pdf.

Dow J.M., Neilan R.E. and Gendt G.; 2009: *The international GNSS service in a changing landscape of global navigation satellite systems*. J. Geod., **83**, 191-198.

Drinkwater M.R., Haagmans R., Muzi D., Popescu A., Floberghagen R., Kern M. and Fehringer M.; 2007: *The GOCE gravity mission: ESA's first core earth explorer*. In: Proc. 3rd Int. GOCE User Workshop, Frascati, Italy, ESA-SP 627, pp. 1-8, ISBN 92-9092-938-3.

EOLI-SA; 2012: *User guide: interacting with earth observation data*. Telespazio France, Toulouse, France, http://earth.esa.int/EOLi/EOLi.htmlhttp://earth.esa.int/EOLi/EOLi.html.

ESA; 1999: *Gravity field and steady-state ocean circulation mission*. European Space Agency, SP-1233(1), 217 pp.

ESA; 2011a: *GOCE L1b data quality control report January 2011*. ESA/ESRIN, Frascati, Italy, Tech. Rep. Issue 1.0.

ESA; 2011b: *GOCE L1b data quality control report SSTI anomaly*. ESA/ESRIN, Frascati, Italy, Tech. Rep. Issue 1.0.

ESA; 2012a: *GOCE L1b data quality control report February 2010*. ESA/ESRIN, Frascati, Italy, Tech. Rep. Issue 2.0.

ESA; 2012b: *GOCE L1b data quality control report July 2010*. ESA/ESRIN, Frascati, Italy, Tech. Rep. Issue 2.0.

ESA; 2012c: *GOCE L1b data quality control report September 2010*. ESA/ESRIN, Frascati, Italy, Tech. Rep. Issue 2.0.

ESA/ESOC; 2009: *NAPEOS - Mathematical models and algorithms, DOPS-SYS-TN-0100-OPS-GN*. European Space Agency, Darmstadt, Germany.

ESA/ESOC; 2013: ftp://dgn6.esoc.esa.int/napeos/ftp://dgn6.esoc.esa.int/napeos/

Förste C., Bruinsma S., Shako R., Marty J.-C., Flechtner F., Abrikosov O., Dahle C., Lemoine J.-M., Neumayer K.H., Biancale R., Barthelmes F., König R. and Balmino G.; 2011: *EIGEN-6 - A new combined global gravity field model including GOCE data from the collaboration of GFZ-Potsdam and GRGS-Toulouse*. In: Proc. General Res. Eur. Geosci. Union, Vienna, Austria, Geophys. Res. Abstr. Vol. 13, EGU2011-3242-2.

GOCE; 2013: *Monthly statistics website*. http://earth.eo.esa.int/missions/goce/monthly/.

GOCE SSTI-A ANTEX; 2013: https://earth.esa.int/web/guest/missions/.

ICGEM; 2013: http://icgem.gfz-potsdam.de/ICGEM/.

IGS; 2013a: *Products*. Website, http://igscb.jpl.nasa.gov/components/prods.html.

IGS; 2013b: *Final Products*. Ftp website, ftp://cddis.gsfc.nasa.govftp://cddis.gsfc.nasa.gov.

Jäggi A., Dach R., Montenbruck O., Hugentobler U., Bock H. and Beutler G.; 2009: *Phase center modeling for LEO GPS receiver antennas and its impact on precise orbit determination*. J. Geod., **83**, 1145-1162, doi:10.1007/s00190-009-0333-2.

Lyard F., Lefevre F., Letellier T. and Francis O.; 2006: *Modelling the global ocean tides: modern insights from FES2004*. Ocean Dyn., **56**, 394-415, doi:10.1007/s10236-006-0086-x.

McCarthy D.D. and Petit G. (eds); 2003: *IERS Conventions (2003), IERS Technical Note n. 32*. Verlag des Bundesamts für Kartographie und Geodäsie, Frankfurt am Main, Germany, ISBN 3-89888-884-3.

Visser P.N.A.M., van den Ijssel J., van Helleputte T., Bock H., Jäggi A., Beutler G. and Heinze M.; 2010: *Rapid and precise orbit determination for the GOCE satellite*. In: Proc. ESA Living Planet Symp., Bergen, Norway, ESA-SP 686, ISBN 978-92-9221-250-6, ISSN 1609-042X, pp. 1-6.

Visser P.N.A.M., van den IJssel J., van Helleputte T., Bock H., Jäggi A., Beutler G., Svehla D., Hugentobler U. and Heinze M.; 2009: *Orbit determination for the GOCE satellite*. Adv. Space Res., **43**, 760-768, doi:10.1016/j.asr.2008.09.016.

Corresponding author: Stefano Casotto
Dip. Fisica e Astronomia, Università di Padova
Via dell'Osservatorio 3, 35122 Padova, Italy
Phone: +39 049 8278224; fax +39 049 8278212; e-mail: stefano.casotto@unipd.it